Entangling Quantum-Logic Gate Operated with an Ultrabright Semiconductor Single-Photon Source

O. Gazzano,[1] M. P. Almeida,[2,3] A. K. Nowak,[1] S. L. Portalupi,[1] A. Lemaître,[1] I. Sagnes,[1] A. G. White,[2,3] and P. Senellart[1,*]

[1]*Laboratoire de Photonique et de Nanostructures, CNRS, UPR20, Route de Nozay, 91460 Marcoussis, France*

[2]*Centre for Engineered Quantum Systems, School of Mathematics and Physics, University of Queensland, Brisbane QLD 4072, Australia*

[3]*Centre for Quantum Computer and Communication Technology, School of Mathematics and Physics, University of Queensland, Brisbane QLD 4072, Australia*

(Received 1 March 2013; published 17 June 2013)

We demonstrate the unambiguous entangling operation of a photonic quantum-logic gate driven by an ultrabright solid-state single-photon source. Indistinguishable single photons emitted by a single semiconductor quantum dot in a micropillar optical cavity are used as target and control qubits. For a source brightness of 0.56 photons per pulse, the measured truth table has an overlap with the ideal case of $68.4 \pm 0.5\%$, increasing to $73.0 \pm 1.6\%$ for a source brightness of 0.17 photons per pulse. The gate is entangling: At a source brightness of 0.48, the Bell-state fidelity is above the entangling threshold of 50% and reaches $71.0 \pm 3.6\%$ for a source brightness of 0.15.

DOI: 10.1103/PhysRevLett.110.250501 PACS numbers: 03.67.Lx, 03.67.Bg, 42.50.Pq, 85.35.Be

The heart of quantum information processing is entangling separate qubits by using multiqubit gates: The canonical entangling gate is the controlled-NOT (CNOT) gate, which flips the state of a target qubit depending on the state of the control. A universal quantum computer can be built by using solely CNOT gates and arbitrary local rotations [1], the latter being trivial in photonics. In 2001, Knill, Laflamme, and Milburn demonstrated that photonic multiqubit gates could be implemented by using only linear-optical components and projective measurements and feedforward [2]. Since then, many schemes to implement linear-optical CNOT gates have been theoretically proposed [3–5] and experimentally demonstrated [6–12]. These demonstrations all used parametric down-conversion as photon sources; however, such sources are not suitable for scalable implementations due to their inherently low source brightness—10^{-6} to 10^{-4} photons per excitation pulse—and contamination with a small but significant multiple-photon component [13–15].

Semiconductor quantum dots (QDs) confined in micropillar optical cavities are close to ideal as photon sources, emitting pulses containing one and only one photon, with high efficiency and brightness. QDs have been shown to emit single photons [16], indistinguishable photons [17], and entangled photon pairs [18,19]. Intrinsically, the QDs emit photons isotropically: Both tapered single mode waveguides [20] and micropillar cavities [21,22] have enabled the fabrication of single-photon sources with brightness of $\sim$0.8 photons per pulse. In the latter case, the Purcell effect further allows reducing the dephasing induced by the solid-state environment, yielding photons with a large degree of indistinguishability [17,22,23].

Very recently, quantum dot single-photon sources have been used to drive linear-optical entangling gates: on a semiconductor waveguide chip, where the truth table was measured [24], and in bulk polarization optics [25], where the gate process fidelity was bounded by measurements in two orthogonal bases [26]. These are necessary, but not sufficient, measurements for unambiguously establishing entanglement [27]; e.g., a CNOT gate has the same truth table as a classical, reversible-XOR gate.

Here we show the unambiguous operation of an entangling CNOT gate using single photons emitted by a single quantum dot deterministically coupled to the optical mode of a pillar microcavity. The source is operated at a remarkably high brightness—above 0.65 collected photons per pulse—and successively emitted photons present a mean wave-packet overlap [17] between 50% and 72%. Bell-state fidelities above 50% are an unimpeachable entanglement witness [27]: We see fidelities up to $71.0 \pm 3.6\%$.

Our source was grown by molecular beam epitaxy and consists of an InGaAs annealed QD layer between two Bragg reflectors with 16 (36) pairs for the top (bottom) mirror. After spin coating the sample with a photoresist, low temperature *in situ* lithography is used to define pillars deterministically coupled to single QDs [28]. We first select QDs with optimal quantum efficiency and appropriate emission wavelength to be spectrally matched to 2.5 μm diameter pillar cavities. A green laser beam is used to expose the disk defining the pillar centered on the selected QD with 50 nm accuracy. To operate the source close to maximum brightness and maintain a reasonably high degree of indistinguishability, we use a two-color excitation scheme. A 905 nm, 82 MHz pulsed laser resonant to an excited state of the QD is used to saturate the QD transition, while a low power continuous-wave laser at 850 nm is used to fill traps in the QD surrounding. This ancillary excitation, giving rise to less than 10% of the signal, reduces the fluctuations of the electrostatic

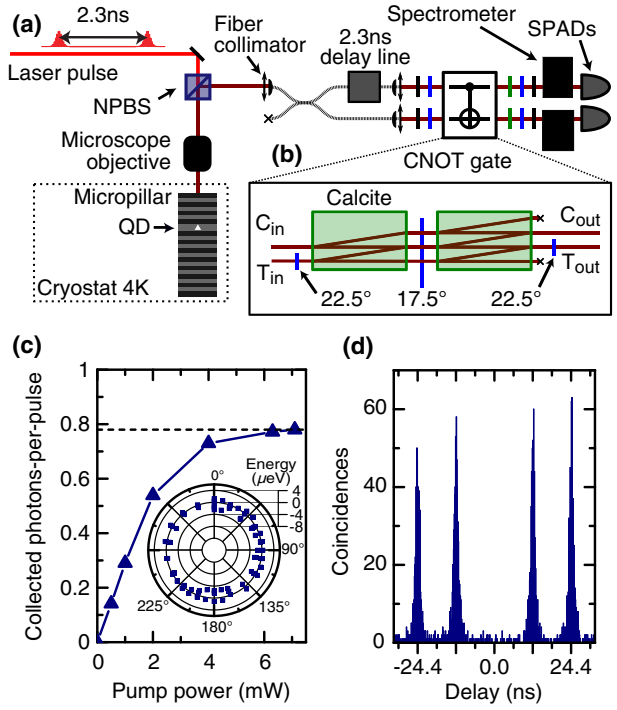

FIG. 1 (color online). (a) Experimental schematic. Single photons are produced by a QD in a micropillar optical cavity, excited by two consecutive laser pulses at 905 nm, temporally separated by 2.3 ns. The cavity is also illuminated by an 850 nm laser to reduce electrostatic fluctuations. A nonpolarizing beam splitter reflecting 90% of the QD signal at 930 nm is employed to send the QD emission into a single-mode fiber and to the input of the CNOT gate. Polarizers (black lines), half- (blue lines), and quarter- (green lines) wave plates are used for state preparation and analysis. The photons are spectrally filtered by two spectrometers and detected by single-photon avalanche photon diodes (SPADs). (b) Experimental schematic of the CNOT gate, as described in Ref. [6]. (c) Collected photons per pulse as a function of the pump power. Inset: Variation of the emission line energy as a function of the polarization angle. (d) Autocorrelation function measured on the QD exciton line.

environment; further details are in Ref. [22]. Our source has a maximum brightness of 0.79 photons per excitation pulse [Fig. 1(c)], as measured in the first collection lens.

The QD emission is collected by a microscope objective with a numerical aperture of 0.4 and coupled to a single-mode fiber with a 70% efficiency, estimated by comparing the measured single-photon count rate with and without fiber coupling. The typical spectrum of the source presents a single emission line around ~930 nm [22]. To characterize the purity of the single-photon emission, we measure the second-order correlation function g^2, by using a Hanbury Brown–Twiss setup [29]. Figure 1(d) shows the measured autocorrelation function under pulsed excitation only, i.e., without the 850 nm laser. Without background correction, we obtain $g^2(0) = 0.01 \pm 0.01$. For the QD under study, the fine structure splitting of the exciton line is below 2 μeV [30] as shown in the inset in Fig. 1(c) presenting the variation of the exciton line energy as a function of the polarization angle. Thanks to the enhancement of spontaneous emission by the Purcell factor $F_p = 3.8$, the photons are indistinguishable in any polarization basis as demonstrated in Ref. [22] by using the Hong-Ou-Mandel experiment. In the following, we operate the source at a brightness of 0.75 collected photon per pulse for measuring the gate truth table and at a brightness of 0.65 for demonstrating two-photon entanglement.

To generate the target and control input photons, the source is excited twice every 12.2 ns—the repetition rate of the laser—with a delay between the two excitations of 2.3 ns. The two photons are nondeterministically separated into two spatial modes by coupling the source to a 50-50 fiber beam splitter; they are brought back into temporal coincidence by adding a 2.3 ns delay line to one of the paths. We implement the CNOT gate following the design of Ref. [6], which requires both classical and quantum multipath interferences [Fig. 1(b)]. The logical qubits are encoded on the polarization state of the photons with $|0\rangle \equiv |H\rangle$ and $|1\rangle \equiv |V\rangle$. We initialize with polarizers and set the gate input state by using half-wave plates. Half-wave plates on the control input and output act as Hadamard gates. Two calcite crystals are used to transform polarization encoding into path encoding. The internal half-wave plate implements the three $1/3$ beam splitters at the heart of this gate [6]. The wave plates and polarizers on the output modes enable analysis in any polarization basis. For spectral filtering, the gate outputs are coupled to spectrometers and are detected via single-photon avalanche photodiodes with 350 ps time resolution.

To obtain the truth table, we measured the output of the gate for each of the four possible logical basis input states $\{|HH\rangle, |HV\rangle, |VH\rangle, |VV\rangle\}$, where $|ct\rangle$ are the control and target qubit states. Figure 2(a) presents a typical experimental pulsed correlation histogram (blue). Every 12.2 ns, a set of five peaks is observed: Each peak corresponds to one of the five possible paths followed by the two photons generated with a 2.3 ns delay. The central peak, cross-hatched area at zero delay, corresponds to events where both the control and target photons enter the gate simultaneously. We will hereafter refer to the five central peaks centered at zero delay as *correlated peaks* and the set of peaks centered at $p \times 12.2$ ns ($p \in \mathbb{Z}^*$) as *uncorrelated peaks*. For each set of peaks, we also define five time bins of tunable width, separated by 2.3 ns, in order to temporally analyze the time evolution of the signal: The time bins for the uncorrelated peaks are shown in gray and, for the correlated peaks, in orange. To evaluate the gate properties, we measure the area of the peaks for a given time-bin size, which we varied between 0.256 and 2 ns. Because the emission decay time of the source is 750 ps, adjacent peaks slightly temporally overlap on the order of 5%–10%. The experimental data presented hereafter are corrected for this overlap (see Supplemental Material [31]).

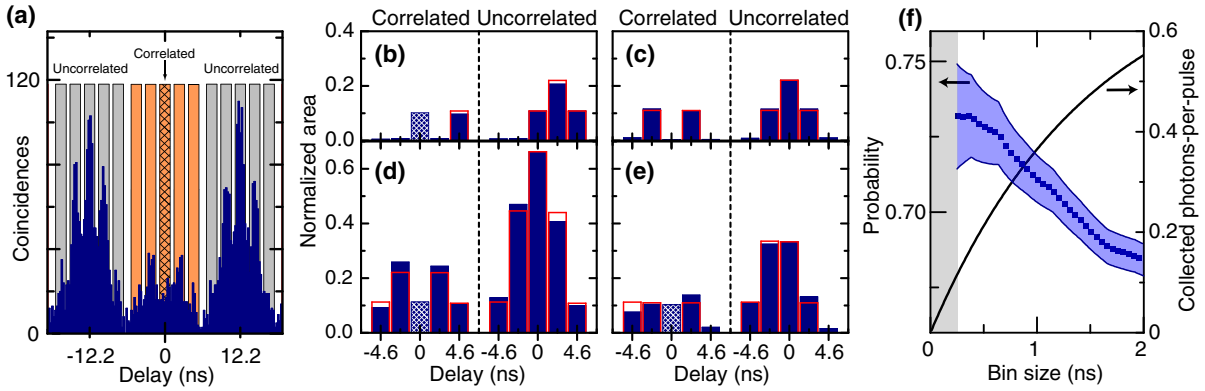

FIG. 2 (color online). (a) Example of a correlation histogram, measured at the output of the CNOT gate for input state $|\psi_{in}\rangle = |1, 1\rangle \equiv |V, V\rangle$ and output state $|\psi_{out}\rangle = |1, 0\rangle \equiv |V, H\rangle$. (b)–(e) Normalized peak areas as a function of time delay or a time bin width of 1 ns: correlated peaks at left, uncorrelated peaks at right (blue bars). Red lines are theoretical predictions. For the input $|0, 1\rangle \equiv |H, V\rangle$, we show the correlation measurements in the basis (b) $|0, 1\rangle \equiv |H, V\rangle$ and (c) $|1, 1\rangle \equiv |V, V\rangle$. For the input $|1, 0\rangle \equiv |V, H\rangle$, we show the correlation measurements in the basis (d) $|1, 0\rangle \equiv |V, H\rangle$ and (e) $|1, 1\rangle \equiv |V, V\rangle$. (f) As a function of time-bin width: (left ordinate) Overlap between measured and ideal truth table for a CNOT gate [27], and (right ordinate) collected photons per pulse.

Figures 2(b) and 2(c) present the measured area of the correlated and uncorrelated peaks, respectively, when the control qubit is set to $|0\rangle$. For this case, the target and control photons do not interfere: The result of the measurement depends only on the purity of the single-photon source $g^2(0)$. In Figs. 2(d) and 2(e), the control qubit is set to $|1\rangle$: Now, the signal measured on the output depends on two-photon interference. For perfectly indistinguishable photons, the peak at zero delay in Fig. 2(d) should completely vanish, whereas it is expected to present the same area as the adjoining peaks at ± 2.3 ns for perfectly distinguishable photons. Our observation of an intermediate case highlights the nonunity indistinguishability of the successively emitted photons. All nonzero delay peaks provide information about the classical interferences occurring inside the gate. The expected areas of those peaks are calculated by considering the optical path followed by nontemporally overlapping photons with Poisson statistics [red lines in Figs. 2(b)–2(e)]. The experimental results (blue bars) are obtained by normalizing the experimental counts—such as those in Fig. 2(a)—by the averaged area of the central uncorrelated peaks, located at $p \times 12.2$ ns, averaged over $p = 1$ to $p = 200$. A close agreement is found between the measurements and ideal case as seen in Figs. 2(b)–2(e).

This procedure allows us to measure output probabilities per input pulse, as shown in Table I for a time-bin width of 1 ns. In the eight logical configurations indicated by α and β, there is actually no signal on one of the detectors: The dark count to signal ratio leads to $\alpha < 0.005$ and $\beta < 0.01$. Using a photon mean wave-packet overlap M of 50%, we see that the measured configurations (Table I) are in very good agreement with those predicted for an ideal gate (Table II) [4]. The value of M is not corrected for imperfections in the experimental setup—such as visibility of the single-photon interference, polarization ratio of the calcite, etc.—and is therefore a lower bound to the source indistinguishability and compares well with previously reported values [22].

The left ordinate of Fig. 2(f) plots the overlap between the measured and ideal CNOT gate truth tables—defined as the probability to obtain the correct output averaged over all possible four inputs [27]—as a function of time-bin width. The right ordinate of Fig. 2(f) shows the number of collected photons per pulse, given by $I_{max} \int_0^{t_{bin}} e^{-t/\tau} dt / \int_0^{\infty} e^{-t/\tau} dt$, where I_{max} is the source operation brightness—here, $I_{max} = 0.75$ collected photons per pulse—and $\tau = 750$ ps is the decay time of the single-photon emission. Figure 2(f) shows that the overlap between the measured and ideal truth

TABLE I. Measured output probabilities per input pulse P, where $P = (1/9)p^*$. Input $|\psi_{in}\rangle = |\text{control, target}\rangle$ qubit states are indicated in the left column. $\alpha < 0.005$ and $\beta < 0.01$.

Input	$p^*_{\|HH\rangle}$	$p^*_{\|HV\rangle}$	$p^*_{\|VH\rangle}$	$p^*_{\|VV\rangle}$
$\|HH\rangle$	1.12(9)	α	0.01(1)	α
$\|HV\rangle$	α	0.97(8)	α	0.04(2)
$\|VH\rangle$	β	α	$2 \times 0.50(6)$	0.92(9)
$\|VV\rangle$	α	β	0.75(9)	$2 \times 0.50(7)$

TABLE II. Ideal output probabilities per input pulse P as a function of mean wave-packet overlap M. Note that the probability is $P = (1/9)p^*$. Input $|\psi_{in}\rangle = |\text{control, target}\rangle$ qubit states are indicated in the left column.

Input	$p^*_{\|HH\rangle}$	$p^*_{\|HV\rangle}$	$p^*_{\|VH\rangle}$	$p^*_{\|VV\rangle}$
$\|HH\rangle$	1	0	0	0
$\|HV\rangle$	0	1	0	0
$\|VH\rangle$	0	0	$2 \times (1\text{-}M)$	1
$\|VV\rangle$	0	0	1	$2 \times (1\text{-}M)$

table increases from 0.684 ± 0.005 for a brightness of 0.56 to 0.730 ± 0.016 when reducing the time bin, thanks to improved indistinguishability of photons emitted at a shorter delay [23,32].

To certify that this gate and source combination can produce entangled states from unentangled inputs, we measure the fidelity of the output state with an ideal Bell state. By setting the control qubit to $|D\rangle = (|V\rangle + |H\rangle)/\sqrt{2}$ and the target qubit to $|H\rangle$, the output of an ideal gate is $\Phi^+ = (|V, V\rangle + |H, H\rangle)/\sqrt{2}$. To measure the fidelity of the experimentally generated state, we measure the polarization of the correlation in three bases [27,33]:

$$E_{\alpha,\beta} = \frac{A_{\alpha,\alpha} + A_{\beta,\beta} - A_{\alpha,\beta} - A_{\beta,\alpha}}{A_{\alpha,\alpha} + A_{\beta,\beta} + A_{\alpha,\beta} + A_{\beta,\alpha}},$$

where $A_{\beta,\alpha}$ is the zero delay peak area measured for the output control photon detected in β polarization and the output target photon in α polarization. The fidelity to the Bell state is then given by $F_{\Phi^+} = (1 + E_{H,V} + E_{D,A} - E_{R,L})/4$, where the antidiagonal polarization is $|A\rangle = (|H\rangle - |V\rangle)/\sqrt{2}$ and the circular basis polarizations are right, $|R\rangle = (|H\rangle + i|V\rangle)/\sqrt{2}$, and left, $|L\rangle = (|H\rangle - i|V\rangle)/\sqrt{2}$. Figures 3(a)–3(f) show the measured correlation curves for two polarization configurations in each basis. As in Fig. 2, the area of the nonzero delay peaks is calculated by considering classical interferences of nontemporally overlapping photons (red lines) and is used to extract the area of the zero delay peak (cross-hatched area).

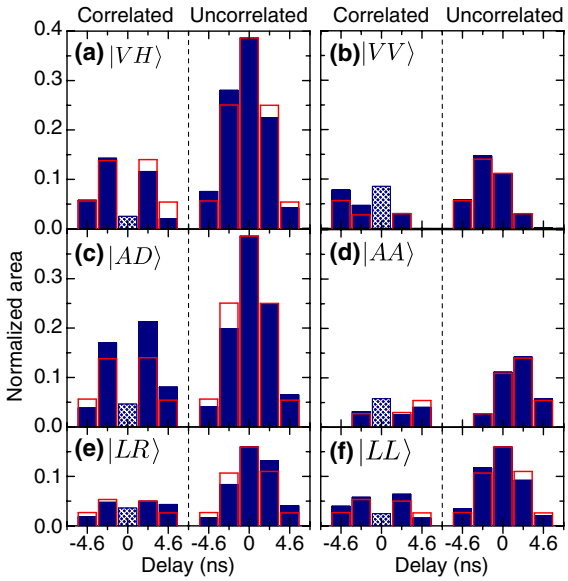

FIG. 3 (color online). (a–f) Area of the correlation peaks as a function of time delay for the correlated peaks (left) and uncorrelated peaks (right) for a time bin of 1 ns (blue bars). Red lines are theoretical predictions. For all measurements the input state is $|D, H\rangle$. The measured output stated are the following: (a) $|V, H\rangle$; (b) $|V, V\rangle$; (c) $|A, D\rangle$; (d) $|A, A\rangle$; (e) $|L, R\rangle$; and (c) $|L, L\rangle$.

Note that, for both linear and diagonal bases, the results of the measurement depend on the two-photon quantum interference only when the output photons are in $|V, H\rangle$, $|V, V\rangle$, $|A, D\rangle$, or $|A, A\rangle$. The four other terms result only from single-photon interferences (not shown).

Figure 4(a) presents the fidelity to the Bell state F_{Φ^+} as a function of time bin. For all time bins, the fidelity to the Bell state is above the 0.5 limit for quantum correlations. For these entanglement measurements, we have only slightly decreased the source brightness, $I_{\max} = 0.65$, in order to obtain a better degree of indistinguishability [22]. Our results show the creation of an entangled two-photon state for a source brightness as large as 0.48 collected photons per pulse. When reducing the time bin to select photons presenting a higher degree of indistinguishability [32], the fidelity increases up to 0.710 ± 0.036, while the source brightness decreases as indicated in the right ordinate of Fig. 4(a).

Figure 4(b) presents the expected fidelity to the Bell state as a function of the mean wave-packet overlap M. Following Ref. [4] to calculate the output coincident count rate for all bases configurations, it can be shown that $F_{\Phi^+} = (1 + M)/[2(2 - M)]$. For $M = 0$, the fidelity is 0.25, which is the value experimentally observed for the uncorrelated peaks (square). For a time bin of 2 ns, the measured fidelity of 0.5 is consistent with $M = 0.5$ (circle), which is a lower bound for M, since our modeling does not take into account the setup experimental imperfections. For a time bin of 400 ps, the measured fidelity of 0.71 shows a mean wave-packet overlap larger than $M = 0.76$ (triangle).

In conclusion, we have demonstrated the successful implementation of an entangling CNOT gate operating with an ultrabright single-photon source. The gate is entangling for all source brightnesses under 0.48, reaching a Bell-state fidelity of $71.0 \pm 3.6\%$ at a source brightness of 0.15 collected photons per pulse. To improve the fidelity of

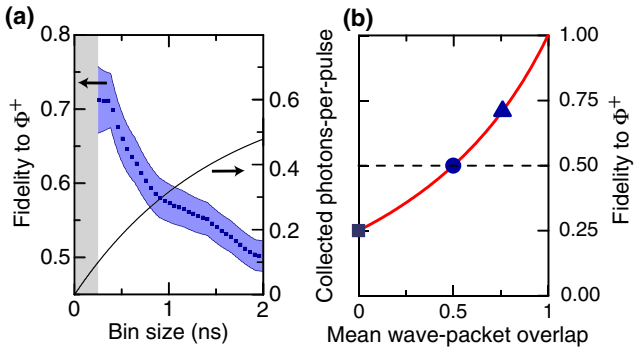

FIG. 4 (color online). (a) Fidelity to the Bell state Φ^+ and number of collected photons per pulse as a function of time bin. (b) Solid line: Calculated fidelity F as a function of the mean wave-packet overlap M. The symbols correspond to the measured fidelity for uncorrelated peaks (square), correlated zero delay peak with a time bin of 2 ns (circle), and a time bin of 400 ps (triangle).

the gate operation while maintaining a high source brightness, one could use an adiabatic design of the micropillar to benefit from a larger Purcell effect to further improve the source indistinguishability [34]. The advances on quantum dot single-photon technologies open exciting possibilities for linear optical computing. Their main asset as compared to heralded single-photon sources based on parametric down-conversion is the possibility to obtain very bright sources as well as negligible multiphoton events. Photonic quantum technologies will require access to multiple single photons, multiplexed in different spatial modes. Small scale implementation of quantum-logic circuits is the first step towards incorporating a quantum-dot-based single-photon source to these technologies.

This work was partially supported by the French ANR P3N DELIGHT, ANR JCJC MIND, the ERC starting Grant No. 277885 QD-CQED, the French RENATECH network, and the CHISTERA project SSQN and the Australia Research Council Centre for Engineered Quantum Systems (CE110001013) and the Centre for Quantum Computation and Communication Technology (CE110001027). O. G. acknowledges support by the French Delegation Generale de l'Armement; M. P. A. by the Australian Research Council Discovery Early Career Award (No. DE120101899) and The University of Queensland Early Career Researcher Grant; and A. G. W. by the University of Queensland Vice-Chancellor's Senior Research Fellowship.

*Corresponding author.
pascale.senellart@lpn.cnrs.fr

[1] M. A. Nielsen and I. L. Chuang, *Quantum Computation and Quantum Information* (Cambridge University Press, Cambridge, England, 2000).
[2] E. Knill, R. Laflamme, and G. J. Milburn, Nature (London) **409**, 46 (2001).
[3] T. C. Ralph, A. G. White, W. J. Munro, and G. J. Milburn, Phys. Rev. A **65**, 012314 (2001).
[4] T. C. Ralph, N. K. Langford, T. B. Bell, and A. G. White, Phys. Rev. A **65**, 062324 (2002).
[5] J. D. Franson, M. M. Donegan, M. J. Fitch, B. C. Jacobs, and T. B. Pittman, Phys. Rev. Lett. **89**, 137901 (2002).
[6] J. L. O'Brien, G. J. Pryde, A. G. White, T. C. Ralph, and D. Branning, Nature (London) **426**, 264 (2003).
[7] T. B. Pittman, M. J. Fitch, B. C. Jacobs, and J. D. Franson, Phys. Rev. A **68**, 032316 (2003).
[8] K. Sanaka, T. Jennewein, J. W. Pan, K. Resch, and A. Zeilinger, Phys. Rev. Lett. **92**, 017902 (2004).
[9] N. Kiesel, C. Schmid, U. Weber, R. Ursin, and H. Weinfurter, Phys. Rev. Lett. **95**, 210505 (2005).
[10] M. Fiorentino and F. N. C. Wong, Phys. Rev. Lett. **93**, 070502 (2004).
[11] R. Okamoto, H. F. Hofmann, S. Takeuchi, and K. Sasaki, Phys. Rev. Lett. **95**, 210506 (2005).
[12] N. K. Langford, T. Weinhold, R. Prevedel, K. J. Resch, A. Gilchrist, J. O'Brien, G. J. Pryde, and A. White, Phys. Rev. Lett. **95**, 210504 (2005).
[13] T. J. Weinhold *et al.*, arXiv:0808.0794.
[14] M. Barbieri, T. J. Weinhold, B. P. Lanyon, A. Gilchrist, K. J. Resch, M. P. Almeida, and A. G. White, J. Mod. Opt. **56**, 209 (2009).
[15] T. Jennewein, M. Barbieri, and A. G. White, J. Mod. Opt. **58**, 276 (2011).
[16] P. Michler, A. Kiraz, C. Becher, W. V. Schoenfeld, P. M. Petroff, L. Zhang, E. Hu, and A. Imamoglu, Science **290**, 2282 (2000).
[17] C. Santori, D. Fattal, J. Vuckovic, G. S. Solomon, and Y. Yamamoto, Nature (London) **419**, 594 (2002).
[18] N. Akopian, N. H. Lindner, E. Poem, Y. Berlatzky, J. Avron, D. Gershoni, B. Gerardot, and P. Petroff, Phys. Rev. Lett. **96**, 130501 (2006).
[19] R. J. Young, R. M. Stevenson, P. Atkinson, K. Cooper, D. A Ritchie, and A. J. Shields, New J. Phys. **8**, 29 (2006).
[20] J. Claudon, J. Bleuse, N. S. Malik, M. Bazin, P. Jaffrennou, N. Gregersen, C. Sauvan, P. Lalanne, and J.-M. Gérard, Nat. Photonics **4**, 174 (2010).
[21] A. Dousse, J. Suffczyński, A. Beveratos, O. Krebs, A. Lemaître, I. Sagnes, J. Bloch, P. Voisin, and P. Senellart, Nature (London) **466**, 217 (2010).
[22] O. Gazzano, S. M. de Vasconcellos, C. Arnold, A. Nowak, E. Galopin, I. Sagnes, L. Lanco, A. Lemaître, and P. Senellart, Nat. Commun. **4**, 1425 (2013).
[23] S. Varoutsis, S. Laurent, P. Kramper, A. Lemaître, I. Sagnes, I. Robert-Philip, and I. Abram, Phys. Rev. B **72**, 041303 (2005).
[24] M. A. Pooley, D. J. P. Ellis, R. B. Patel, A. J. Bennett, K. H. A. Chan, I. Farrer, D. A. Ritchie, and A. J. Shields, Appl. Phys. Lett. **100**, 211103 (2012).
[25] Y.-M. He, Y. He, Y.-J. Wei, D. Wu, M. Atatüre, C. Schneider, S. Höfling, M. Kamp, C.-Y. Lu, and J.-W. Pan, Nat. Nanotechnol. **8**, 213 (2013).
[26] J. L. O'Brien, G. J. Pryde, A. Gilchrist, D. F. V. James, N. K. Langford, T. C. Ralph, and A. G. White, Phys. Rev. Lett. **93**, 080502 (2004).
[27] A. G. White, A. Gilchrist, G. J. Pryde, J. L. O'Brien, M. J. Bremner, and N. K. Langford, J. Opt. Soc. Am. B **24**, 172 (2007).
[28] A. Dousse, L. Lanco, J. Suffczyński, E. Semenova, A. Miard, A. Lemaître, I. Sagnes, C. Roblin, J. Bloch, and P. Senellart, Phys. Rev. Lett. **101**, 267404 (2008).
[29] R. Hanbury Brown and R. Q. Twiss, Nature (London) **177**, 27 (1956).
[30] D. J. P. Ellis, R. M. Stevenson, R. J. Young, A. J. Shields, P. Atkinson, and D. A. Ritchie, Appl. Phys. Lett. **90**, 011907 (2007).
[31] See Supplemental Material at http://link.aps.org/supplemental/10.1103/PhysRevLett.110.250501 for [brief description].
[32] R. M. Stevenson, C. L. Salter, J. Nilsson, A. J. Bennett, M. B. Ward, I. Farrer, D. A. Ritchie, and A. J. Shields, Phys. Rev. Lett. **108**, 040503 (2012).
[33] D. F. V. James, P. G. Kwiat, W. J. Munro, and A. G. White, Phys. Rev. A **64**, 052312 (2001).
[34] M. Lermer, N. Gregersen, F. Dunzer, S. Reitzenstein, S. Höfling, J. Mørk, L. Worschech, M. Kamp, and A. Forchel, Phys. Rev. Lett. **108**, 057402 (2012).